# Entropy Drives Accelerated Ion Diffusion upon Carbon Dioxide-Expansion of Electrolytes

Elizabeth R. Bartlett, Ashley K. Borkowski, Christian K. Nilles, James D. Blakemore, and Ward H. Thompson*

*Department of Chemistry, University of Kansas, Lawrence, KS 66045, USA*

E-mail: wthompson@ku.edu

## Abstract

Carbon dioxide-expanded liquids, organic solvents with high concentrations of soluble carbon dioxide ($CO_2$) at mild pressures, have gained attention as green catalytic media due to their improved properties over traditional solvents. More recently, carbon dioxide-expanded electrolytes (CXEs) have demonstrated improved reaction rates in the electrochemical reduction of $CO_2$, by increasing $CO_2$ delivery to the electrode while maintaining facile charge transport. However, recent studies indicate that a limiting behavior of CXEs at higher $CO_2$ pressures is a decline in solution conductivity due to reduced polarity, leading to poorer charge screening and greater ion pairing. In this Paper, we employ molecular dynamics simulations to investigate the energetic driving forces behind the diffusive properties of an acetonitrile and tetrapropylammonium hexafluorophosphate ($TPrAPF_6$) CXE with increasing $CO_2$ concentration. Our results indicate that entropy drives solvent and electrolyte diffusion with increasing $CO_2$ pressure. The activation energy of ion diffusion increases with higher concentrations of $CO_2$, indicating that increasing temperature may improve solution conductivity in these systems. This trend in the activation energies is traced to stronger cation-anion Coulombic interactions, due to weaker solvent screening at high $CO_2$ concentrations, suggesting that the choice of ion may provide a route to diminish this effect.

## 1 Introduction

Carbon dioxide-expanded liquids (CXLs) are formed by using carbon dioxide ($CO_2$) to pressurize an organic solvent, leading to a volume expansion of the solution.[1,2] These CXLs have significant potential as a versatile and 'green' catalytic reaction media because they possess several qualities that address the drawbacks of traditional reaction media, including reduced viscosity, increased mass transport, and a non-flammable vapor phase.[1–7] Moreover, they represent a route to greener processes as CXLs reduce the amount of organic solvent required while maintaining highly tunable solubility and polarity.[2,4–6]

More recently, these approaches have been expanded to applications in electrochemistry through the development of $CO_2$-expanded electrolytes (CXEs). CXEs can support $CO_2$ concentrations of up to 15 M at relatively mild pressures of $0.7-55.1$ bar,[8] making them highly relevant for $CO_2$ conversion processes. This is particularly advantageous for the electrochemical reduction of $CO_2$, where it removes the, often significant, limitations of $CO_2$ delivery to the electrode.[7,9] While conventional $CO_2$ reduction in aqueous media requires close to ambient operating conditions (at which $CO_2$ concentration is 0.034 M)[10] to avoid acidification,[11–14] CXEs overcome this limitation and achieve higher $CO_2$ reduction rates.[10] CXEs also operate at milder conditions than supercritical $CO_2$,[7,15] which requires pressures ex-

ceeding 74 bar at near ambient temperature.[16] Although numerous experimental and theoretical studies have characterized CXLs, the molecular-level properties of CXEs have received less attention than they deserve.

Recently, Piskulich and Laird conducted molecular dynamics (MD) simulations on an acetonitrile (MeCN)-based CXE with lithium perchlorate salt to assess the impact of electrolyte concentration on $CO_2$ expansion and transport properties of the CXE.[17] In our recent work, we combined experimental and theoretical approaches to quantify solution conductivity with $CO_2$ expansion, addressing a crucial limitation of CXEs: As more nonpolar $CO_2$ molecules are added, the solution conductivity diminishes.[8] We obtained excellent agreement between the experimentally measured solution conductivity and values obtained from MD simulations for a MeCN-based CXE with tetraalkylammonium hexafluorophosphate electrolyte. We found that the decline in solution conductivity at high $CO_2$ pressures is primarily attributable to reduced overall polarity of the solution, which leads to decreased charge screening capacity of the solvent and thereby increased ion pairing.

To develop design principles for CXEs to overcome the limitations of solution conductivity at high $CO_2$ concentrations, a comprehensive, molecular-level understanding of the factors influencing the dynamical properties is needed. In the present work, we address this issue by using our previously developed CXE model[8] to investigate the energetics behind the ion-pairing behaviors that lead to decreased solution conductivity, with the goal of designing CXEs with electrolytes that minimize these interactions. More broadly, a fundamental study of the properties of CXEs with increasing $CO_2$ pressures is valuable for the further development and implementation of these media.

In this study, we investigate the energetics that govern the dynamics of CXEs using MD simulations and fluctuation theory for dynamics.[18–20] These enable an exploration of the activation energy of diffusion over the experimental range of $CO_2$ pressures and, importantly, a decomposition of the activation energy into its contributions from various energetic components and molecular interactions. Furthermore, we investigate the entropic contributions to diffusion, gaining insight into the role of entropy in the diffusion of CXEs with changing $CO_2$ pressure. While solution conductivity is of particular interest for applications of CXEs in electrochemistry, here we consider instead the diffusive behavior of all components of the CXE, which is simpler to interpret. Nevertheless, the strong correlation between diffusion and solution conductivity means that the present investigation reveals the key factors that govern the latter in CXEs.

# 2 Theory

The mean-squared displacement, $MSD_\alpha(t)$, for each species $\alpha$ in the CXE were calculated as

$$MSD_\alpha(t) = \frac{1}{N_\alpha}\sum_{i=1}^{N_\alpha}\langle|\vec{r}_i(t) - \vec{r}_i(0)|^2\rangle, \qquad (1)$$

where $\vec{r}_i(t)$ is the position vector of molecule $i$'s central atom at time $t$ and $N_\alpha$ is the number of molecules of type $\alpha$. The diffusion coefficient, $D_\alpha$, is then calculated from the slope of the corresponding $MSD_\alpha(t)$ as

$$D_\alpha = \lim_{t\to long}\frac{MSD_\alpha(t)}{6t}. \qquad (2)$$

We have previously demonstrated that the activation energy of diffusion can be calculated from simulations at a single temperature using a fluctuation theory for dynamics approach.[19,20] Specifically, it is straightforward to show that the derivative of $MSD_\alpha(t)$ with respect to the inverse temperature, $\beta = 1/k_BT$, is given by

$$\begin{aligned}\frac{\partial MSD_\alpha(t)}{\partial\beta} &= -\frac{1}{N_\alpha}\sum_{i=1}^{N_\alpha}\langle\delta H(0)\,|\vec{r}_i(t) - \vec{r}_i(0)|^2\rangle \\ &\equiv -MSD^H_\alpha(t). \qquad (3)\end{aligned}$$

Here, $H(t)$ is the total system Hamiltonian at time $t$ and $\delta H(0) = H(0) - \langle H\rangle$ is thus the fluctuation in the system energy at time zero from its average value. It then follows that the

diffusion activation energy is given as

$$E_{a,\alpha} = \lim_{t \to long} \frac{MSD^H_\alpha(t)}{MSD_\alpha(t)}. \quad (4)$$

However, in practice, it is more accurate to calculate $E_{a,\alpha}$ from the ratio of the slopes of $MSD^H_\alpha(t)$ and $MSD_\alpha(t)$, and this is the approach we use in the present calculations. Because $MSD^H_\alpha(t)$ measures the correlation between the diffusive dynamics and system energy, it is sensitive to thermostat effects. Thus, we calculate it from an ensemble of constant energy ($NVE$) trajectories initiated from constant temperature ($NVT$) simulations, as described in more detail in Sec. 3.2.

The fluctuation theory for dynamics approach also enables calculation of the contributions to the activation energy of diffusion from the energetic terms that make up the total energy.[19,20] For example, the total energy of a system is the sum of the kinetic ($KE$) and potential ($V$) energies, and therefore so is its fluctuation relative to the average. The potential energy in the present MD simulations can further be represented as a sum of Lennard-Jones ($LJ$), Coulombic ($Coul$), bond ($b$), angle ($ang$), and dihedral ($dih$) contributions. Thus,

$$\begin{aligned} \delta H(0) &= \delta KE(0) + \delta V_{LJ}(0) + \delta V_{Coul}(0) \\ &+ \delta V_b(0) + \delta V_{ang}(0) + \delta V_{dih}(0). \end{aligned} \quad (5)$$

Using this expression in Eqs. (3) and (4) gives a rigorous decomposition of the activation energy of diffusion for a given species $\alpha$ as

$$\begin{aligned} E_{a,\alpha} &= E^{KE}_{a,\alpha} + E^{LJ}_{a,\alpha} + E^{Coul}_{a,\alpha} \\ &+ E^{b}_{a,\alpha} + E^{ang}_{a,\alpha} + E^{dih}_{a,\alpha}. \end{aligned} \quad (6)$$

Similarly, the system energy can be decomposed into contributions from interactions between different types of molecules, *e.g.*, as

$$\begin{aligned} \delta H(0) &= \delta KE(0) + \delta V(0) \\ &= \delta KE(0) + \sum_\gamma \sum_{\zeta > \gamma} \delta V_{\gamma\zeta}(0), \end{aligned} \quad (7)$$

where $\gamma$ and $\zeta$ index the four species in the CXE: MeCN, $CO_2$, tetrapropylammonium ($TPrA^+$), and hexafluorophosphate ($PF_6^-$). This gives a decomposition of the activation energy as

$$E_{a,\alpha} = E^{KE}_{a,\alpha} + \sum_\gamma \sum_{\zeta > \gamma} E^{\gamma\zeta}_{a,\alpha}, \quad (8)$$

which gives the contributions to the diffusion activation energy due to the intermolecular interactions between different molecule types.

These decompositions of the diffusion activation energy are readily interpreted using Tolman's description of the activation energy. He showed that the activation energy for a chemical reaction can be rigorously written as[20–23]

$$E_a = \langle H \rangle_{reacting} - \langle H \rangle_{reactant}. \quad (9)$$

That is, the activation energy at constant volume is the difference in the average (internal) energy of molecules that react and the average (internal) energy of reactants. In this context, a contribution to the diffusion activation energy such as $E^{Coul}_{a,\alpha}$ can be understood as the difference in average Coulombic energy of the molecules that successfully diffuse (*i.e.*, pass over the barrier for diffusion) and the average energy of all molecules. In other words, each contribution tells us how much of that energy is needed for accelerating diffusion. Note that the contributions can be negative so, having greater energy of some types can be detrimental to diffusion.[19]

# 3 Computational Methods

## 3.1 Force Fields

The MeCN molecules were described by the three-site potential developed by Edwards *et al.*, with a united-atom (UA) description of the methyl group.[24] The $CO_2$ molecules were described by the second elementary physical model (EPM2) by Harris and Yung.[25] However, while the MeCN and $CO_2$ bonds were held rigid using the SHAKE algorithm,[26] all other bonds and angles (for these molecules and the ions) were flexible using harmonic potentials. $TPrA^+$ ions were described by the General AMBER force field (GAFF) force field developed

by Wang *et al.*;[27] and $PF_6^-$ ions were described by the UA force field developed by Liu *et al.*[28] The force field bond, angle, dihedral, and nonbonded parameters are given in Tables S1-S4 of the Supporting Information.

### 3.2 Simulation Details

The MD simulations were performed using the Large-scale Atomic/Molecular Massively Parallel Simulator (LAMMPS).[29] Six systems were created to model the CXE at increasing $CO_2$ pressures, corresponding to experimentally determined concentrations of $CO_2$ and electrolyte. In each system, the number of MeCN, $TPrA^+$, and $PF_6^-$ were held constant at 849, 20, and 20, respectively, while the number of $CO_2$ molecules was increased with increasing $CO_2$ pressure. Details of each system are given in Table S5 of the Supporting Information. Fig. 1 provides a visualization of the changing system composition and demonstrates the volumetric expansion of the CXE; the solution volume increases by a factor of more than 2.5 from 3.4 to 51.0 bar.

For each system, five $NVT$ simulations were run for 2 ns equilibration and 5 ns production stages at 298.15 K. For the larger systems ($CO_2$ pressures of 44.8 and 51.0 bar), the production runs were propagated for 25 ns. In all simulations, a cutoff of 10.0 Å was applied to both Lennard-Jones and Coulombic interactions. Tail corrections to the Lennard-Jones interactions were applied, and a particle-particle-particle mesh Ewald with a tolerance of $1 \times 10^{-4}$ was used to describe the long-range electrostatics.[31,32] A Nosé-Hoover thermostat was used to maintain temperature during all constant temperature simulations using a 100 fs damping parameter.[33,34]

From configurations extracted every 1 ps from the $NVT$ production runs, $NVE$ trajectories were propagated for 20 ps with positions and momenta written every 50 fs. There were 25,000 total $NVE$ trajectories for each system at lower pressures and 125,000 total $NVE$ trajectories for the larger systems at higher pressures. The timestep in all simulations was 1 fs. All dynamical properties (see Sec. 2) are calculated from the $NVE$ trajectories. Slopes of the $MSD_\alpha(t)$ and $MSD_\alpha^H(t)$ in the calculation of $D_\alpha$ and $E_{a,\alpha}$ in Eqs. (3) and (4) were taken from linear fits over $5-20$ ps. Errors in the computed values were calculated using block averaging over 5 blocks and were reported as 95% confidence intervals using Student's $t$-distribution.[35]

## 4 Results

We first consider the diffusion coefficients of each species in the CXE as a function of increasing $CO_2$ pressure. The results are presented in Fig. 2 and show that, as $CO_2$ pressure increases, the diffusion coefficient for every species increases. However, the effect is greater for $CO_2$ and MeCN compared to the ions. Because the volumetric expansion of the CXE is nonlinear, we plot the data as a function of electrolyte concentration; the number of ions in the simulations is constant, so this axis is proportional to the inverse of the solution volume. On this scale, the increase in the MeCN diffusion coefficient is effectively linear with the decrease of the salt concentration. On the other hand, $D_{CO_2}$ increases in a more rapid, nonlinear fashion and both ionic species first show an initial increase as the solution becomes more dilute before plateauing. These increased mobilities coincide with a decrease in the shear viscosity of the solution as more $CO_2$ is added, as we have previously shown.[8] In this context, it is important to note that the $CO_2$ concentration in the system is also increasing nonlinearly, indicating that the $CO_2$ mobility is enhanced by the greater fraction of like molecules in the solution.

We previously calculated the solution conductivity of the CXE over the range of $CO_2$ pressures considered here and demonstrated excellent agreement with experimental measurements.[8] The solution conductivity depends on the diffusion coefficients of the electrolytes (which is considered here) as well as the correlated motion of the ions (which is not). The ability of the simulation model to accurately predict solution conductivity trends gives confidence that it provides a good representation

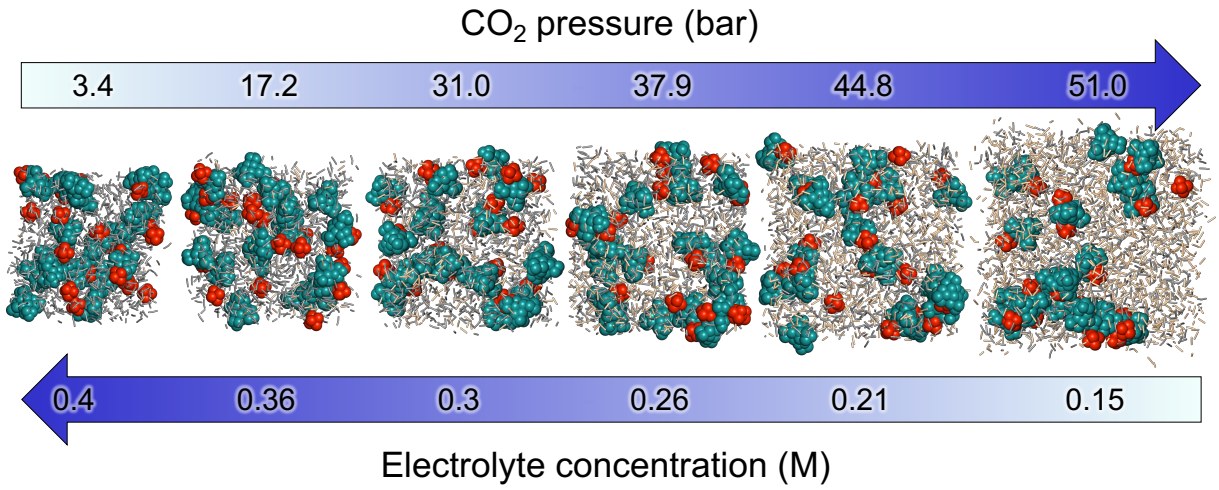


Figure 1: CXE systems with increasing $CO_2$ pressure and corresponding electrolyte dilution, depicting MeCN (gray), $CO_2$ (tan), $TPrA^+$ (teal), and $PF_6^-$ (red). System visualizations were prepared using PyMOL.[30]

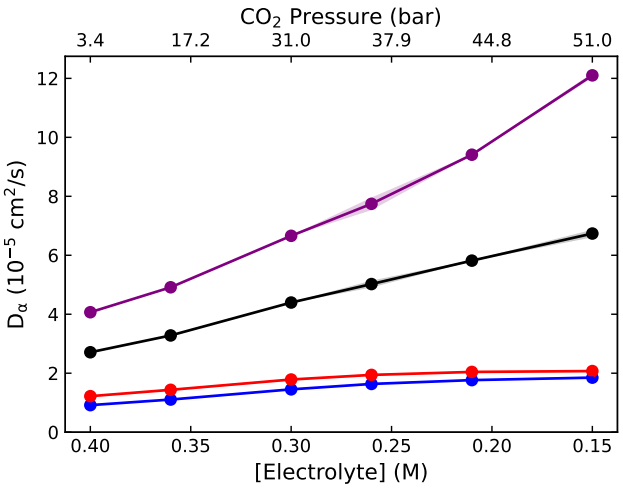


Figure 2: Diffusion coefficient of each type of molecule in the CXE system as a function of the electrolyte concentration, as modified by dilution due to $CO_2$ pressure. Results are shown for $CO_2$ (purple), MeCN (black), $PF_6^-$ (red), and $TPrA^+$ (blue). Shaded regions indicate 95% confidence intervals.

of the diffusive properties of the system.

Nevertheless, it is useful to compare the present diffusion coefficients with prior measurements and calculations. For example, we find that the MeCN diffusion coefficient at the lowest $CO_2$ composition ($D_{MeCN} = (2.710 \pm 0.003) \times 10^{-5}$cm$^2$/s) is substantially lower than the $(4.12 - 5.0) \times 10^{-5}$cm$^2$/s measured in bulk acetonitrile.[36] However, in MD simulations using the same MeCN model, $D_{MeCN}$ has been reported as $(3.1 - 3.4) \times 10^{-5}$ cm$^2$/s in the neat liquid.[37,38] These results indicate that the presence of the ions is inhibiting diffusion of MeCN. While CXEs have not been extensively studied, ionic liquids diluted with MeCN have similar characteristics and are a valuable point of comparison for the mobility of the ions. In 1.6 M ethylammonium nitrate in MeCN, $D_{cation}$ was measured as $0.799 \times 10^{-5}$ cm$^2$/s.[39] In 1.5 M tetraethylammonium tetrafluoroborate in MeCN, $D_{cation}$ and $D_{anion}$ were measured as $(1.49 \pm 0.08) \times 10^{-5}$ cm$^2$/s and $(1.65 \pm 0.03) \times 10^{-5}$ cm$^2$/s, respectively.[40] These systems have smaller cations and anions as well as ion concentrations significantly greater than our most concentrated, 0.4 M, CXE conditions. However, with these competing effects, the diffusion coefficients are on the same order as our results, where $D_{TPrA^+} = (0.917 \pm 0.007) \times 10^{-5}$ cm$^2$/s and $D_{PF_6^-} = (1.221 \pm 0.008) \times 10^{-5}$ cm$^2$/s.

Next we consider the activation energies of diffusion for the different species using the fluctuation theory approach described in Sec. 2. Fig. 3 shows that the activation energy of diffusion grows with increasing $CO_2$ pressure for MeCN, $PF_6^-$, and $TPrA^+$, but decreases for $CO_2$. This is a striking result because it

shows that, as the solution is expanded by $CO_2$, the mobilities of MeCN and the ions increase (Fig. 2) despite increases in the corresponding activation energies. This implicates a strong, even determinative, entropic contribution to diffusion of MeCN and ions, particularly at high pressures of $CO_2$. This is examined in detail below in Sec. 5.1.

At 3.4 bar, the diffusion activation energy is the same (within error) for all species at around $E_{a,\alpha} = 4.44 - 5.44$ kJ/mol. The system at this pressure is most comparable to neat MeCN for which we previously found $E_{a,MeCN} = 4.81$ kJ/mol from an Arrhenius analysis,[41] though using a different force field.[42] We note, however, that Hurle and Woolf carried out temperature-dependent measurements of the self-diffusion of MeCN in the neat liquid[43] and, while they did not report the activation energy, their data yields $E_{a,MeCN} = 8.62$ kJ/mol. The origin of this discrepancy is unclear, but may be associated with the MeCN force fields or, in the present case, the effect of the ions.

Piskulich and Laird also calculated the diffusion activation energy for MeCN and $CO_2$ using fluctuation theory methods for a CXE system with MeCN solvent and lithium perchlorate electrolyte.[17] Their system at 20 bar is most comparable in terms of electrolyte and $CO_2$ composition to our system at 17.2 bar. At these conditions, they found $E_{a,MeCN} = 4.02 \pm 0.21$ kJ/mol and $E_{a,CO_2} = 4.60 \pm 0.42$ kJ/mol, compared to our results of $E_{a,MeCN} = 4.56 \pm 0.25$ kJ/mol and $E_{a,CO_2} = 3.85 \pm 0.46$ kJ/mol. These results use the same MeCN model and again show excellent agreement to our results, while the minor differences may be attributed to the differences in electrolyte identity and system composition at the different pressures.

The maximum values of the activation energies of diffusion for MeCN, $TPrA^+$, and $PF_6^-$ at 51.0 bar are also statistically the same at around $9.75 - 10.67$ kJ/mol. This indicates that the diffusion of these three species are intricately related in the CXE. At the same pressure, the $CO_2$ diffusion activation energy reaches its lowest value of $2.47 \pm 0.38$ kJ/mol.

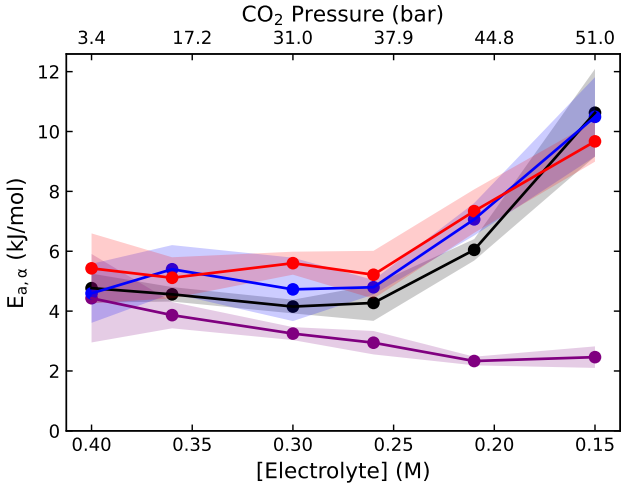


Figure 3: Activation energy of diffusion of each type of molecule in the CXE system with increasing $CO_2$ pressure/corresponding electrolyte dilution for $CO_2$ (purple), MeCN (black), $PF_6^-$ (red), and $TPrA^+$ (blue). Shaded regions indicate 95% confidence intervals.

# 5 Discussion

We now shift our focus to a deeper examination of the origins of the the $CO_2$ pressure-dependent behavior of the diffusion coefficients and diffusion activation energies within the CXE system. The CXE undergoes a dramatic change with $CO_2$ expansion. At 3.4 bar, the simulation box has a volume of ~83,000 Å$^3$ and contains just 7 $CO_2$ molecules, while at 51.0 bar, the volume has increased nearly 3-fold and contains 1613 $CO_2$ molecules (see Table S5). At the highest pressure, the CXE is much more nonpolar, and the electrolytes are just below their solubility limit.[8] In understanding and designing such CXE systems, it is critical to understand the driving forces that underlie their tunability *via* $CO_2$ pressure. In this context, we will particularly consider the roles of entropy, ion pairing, and the different interactions present in the system.

## 5.1 Entropy

To elucidate the entropic contribution to diffusion, the relative activation entropy of diffusion was calculated using methods we have previously utilized[44] by describing the diffusion co-

efficient by a transition state theory (TST)-type expression:

$$D(T) \approx D_A e^{-\beta \Delta A^\ddagger} = D_A e^{-\beta \Delta U^\ddagger} e^{\Delta S^\ddagger / k_B}, \quad (10)$$

where $D_A$ is the "attempt frequency" factor which is assumed to be the same at all $CO_2$ pressures, $\Delta A^\ddagger$, $\Delta U^\ddagger$, and $\Delta S^\ddagger$ are the activation Helmholtz free energy, internal energy, and entropy, respectively. The most significant approximation here is taking $D_A$ to be constant when it might reasonably be thought to increase with $CO_2$ concentration as the solution viscosity decreases; it is, however, unlikely that this effect would be of sufficient magnitude to alter the conclusions below. While in TST, these thermodynamic properties depend on a choice of the transition state dividing surface, Tolman's interpretation of the activation energy, Eq. (9), shows that $\Delta U^\ddagger = E_a$ for a hypothetical non-recrossing dividing surface.[20,45] Thus, we can rewrite Eq. (10) for each species $\alpha$ in the CXE at a given $CO_2$ pressure, $p$, as

$$D_\alpha(T,p) \approx D_{A,\alpha} e^{-\beta E_{a,\alpha}(p)} e^{S_{a,\alpha}(p)/k_B}, \quad (11)$$

where we have assumed $D_{A,\alpha}$ is independent of the pressure and defined the activation entropy, $S_{a,\alpha}$, that accompanies the use of the activation energy as the internal energy.

Then, we can find the change in activation entropy as the solution is expanded, relative to the CXE at 3.4 bar, as $\Delta S_{a,\alpha}(p) = S_{a,\alpha}(p) - S_{a,\alpha}(p_0)$, such that

$$\frac{D_\alpha(T,p)}{D_\alpha(T,p_0)} = e^{-\beta \Delta E_{a,\alpha}(p)} e^{\Delta S_{a,\alpha}(p)/k_B}, \quad (12)$$

where $\Delta E_{a,\alpha}(p) = E_{a,\alpha}(p) - E_{a,\alpha}(p_0)$ with $E_{a,\alpha}(p_0)$ and $S_{a,\alpha}(p_0)$ the reference values at $p_0 = 3.4$ bar.

The relative activation entropy of diffusion as a function of $CO_2$ pressure from this calculation is presented in Fig. 4. The ions and MeCN all show similar behavior, where at high $CO_2$ pressures the relative activation entropy of diffusion becomes more favorable, *i.e.*, $\Delta S_{a,\alpha}(p)$ becomes more positive, or $-T\Delta S_{a,\alpha}(p)$ becomes more negative. This demonstrates that at high pressures of $CO_2$, entropy drives the faster diffusion of these molecules. Conversely, $CO_2$ shows no change in the activation entropy of diffusion with changing $CO_2$ pressure. As the activation energy of diffusion decreases with increasing $CO_2$ pressure (Fig. 3), this demonstrates that the faster diffusion of $CO_2$ is driven by a reduction of the energetic barrier as $CO_2$ pressure is increased.

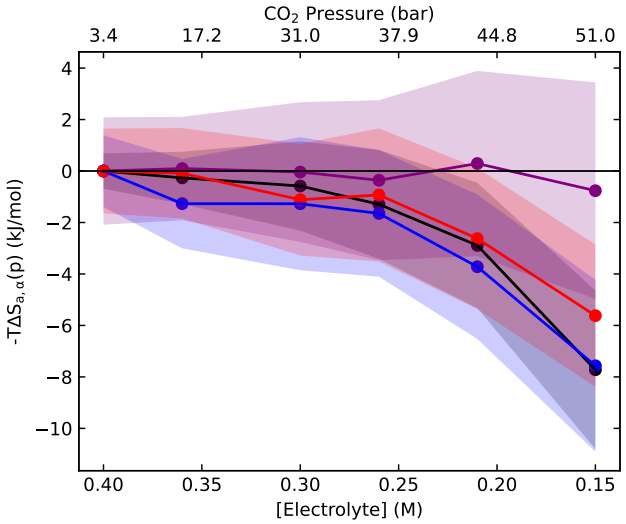


Figure 4: Relative activation entropy of diffusion contribution, $-T\Delta S_{a,\alpha}(p)$, for each type of molecule in the CXE system with increasing $CO_2$ pressure/corresponding electrolyte dilution for $CO_2$ (purple), MeCN (black), $PF_6^-$ (red), and $TPrA^+$ (blue). Shaded regions indicate 95% confidence intervals.

We can also predict diffusion coefficients as a function of $CO_2$ pressures from our calculated activation energies, under the assumption that the entropic contribution to diffusion is invariant with $CO_2$ pressure, by taking $\Delta S_{a,\alpha}(p) = 0$ in Eq. (12). These predicted diffusion coefficients as a function of $CO_2$ pressure are presented in Fig. S1, along with the actual $D_\alpha$ values from Fig. 2. Again, the ions and MeCN show similar behavior, where at low $CO_2$ pressures the predicted diffusion coefficients are within error to the actual values, *i.e.*, entropy has a minimal contribution to diffusion, but at high $CO_2$ pressures, the predicted diffusion coefficients deviate from the actual. This demonstrates that at high pressures, the increasing activation energy of diffusion for the ions and MeCN would lead to decreasing diffusion coef-

ficients if entropic effects were invariant with pressure. In contrast, for $CO_2$, the prediction is in agreement across the pressure range, indicating that entropic factors play a minor role in the diffusion of $CO_2$.

This behavior, in which the diffusion of some species is governed by entropic effects and others by energetic effects, is quite remarkable. The results suggest that higher temperatures could be used to increase the ion (and MeCN) diffusion coefficients, while having a more modest effect on the $CO_2$ behavior. It is important to note, however, that our calculated activation energies are for fixed composition. Raising the temperature will also have the effect of reducing the amount of $CO_2$ in the CXE. Nevertheless, the present results indicate that this may be a fruitful avenue for modulating solution conductivities (and other properties of the electrolyte that we discuss below).

## 5.2 Contributions to the Activation Energies

To understand the origins of the diffusion activation energies shown in Fig. 3 and how they change with the $CO_2$ pressure, we probe the role of different intra- and intermolecular interactions. This is enabled by the fluctuation theory for dynamics approach described in Sec. 2.

Contributions to the activation energy of diffusion with changing $CO_2$ pressure were calculated from Eq. (6) and are presented in Fig. 5. For each molecule, the bond and dihedral potential energy contributions ($E_{a,\alpha}^{bond}$ and $E_{a,\alpha}^{dih}$) were effectively zero at all $CO_2$ pressures, thus the major contributions to the activation energy of diffusion are kinetic energy as well as the Lennard-Jones, Coulombic, and angle bending potential energies. For all molecules, the kinetic energy contribution to the activation energy of diffusion is roughly constant with $CO_2$ pressure and makes up about half of the total $E_{a,\alpha}$ at pressures below 44.8 bar.

The contributions from Lennard-Jones, Coulombic, and angular potential energies all comprise a small positive contribution to the total activation energy of diffusion at the lower pressures. At 44.8 bar, the Lennard-Jones and Coulombic contributions to $E_{a,\alpha}$ increase slightly for MeCN, $TPrA^+$, and $PF_6^-$ while the angular contribution shows a small decrease. The diffusion of $CO_2$ exhibits similar behavior in its angular contribution, but to a lesser degree. These effects are enhanced at 51.0 bar, where the total activation energy has significant contributions from Lennard-Jones and Coulombic potential energies for all molecules and the angular contribution decreases sharply, so that it gives a negative contribution to the total activation energy of diffusion.

The dramatic change in the angular potential energy contribution at 51.0 bar may be associated with the limitations of $CO_2$-expansion in these electrolytes. Experimentally, it is observed that just beyond the highest $CO_2$ pressures considered here, the system develops increased heterogeneity and the ions become no longer soluble.[8] Our results may be reflecting the beginning of longer-ranged ion pairing and the development of larger ionic clusters in the increasingly nonpolar system; this is certainly indicated by the increasing Coulombic and Lennard-Jones contributions to the MeCN and ion activation energies at the highest $CO_2$ pressures. The behavior of $E_{a,\alpha}^{ang}$ may be a manifestation of this structure, with the angular energetics showing a marked difference from those at lower pressures. As the system is mainly composed of $CO_2$ at 51.0 bar (see Table S5), most of the angular potential energy is attributed to the $CO_2$ bond angle (see Fig. S2). Note that a negative $E_{a,\alpha}^{ang}$ contribution means that the angular potential energy is lower at the transition state for diffusion, for $CO_2$ this implies that the molecule must become more linear to enhance diffusion of itself and the other molecule types. This seems to be a reasonable consequence of the higher pressures and the presence of increased ion pairing, but it is not clear why the change is so sharp between 44.8 and 51.0 bar.

## 5.3 Ion-pairing

The limiting behavior of CXEs at high $CO_2$ pressures is a decline in solution conductivity. Structurally, the extent of ion pairing with $CO_2$

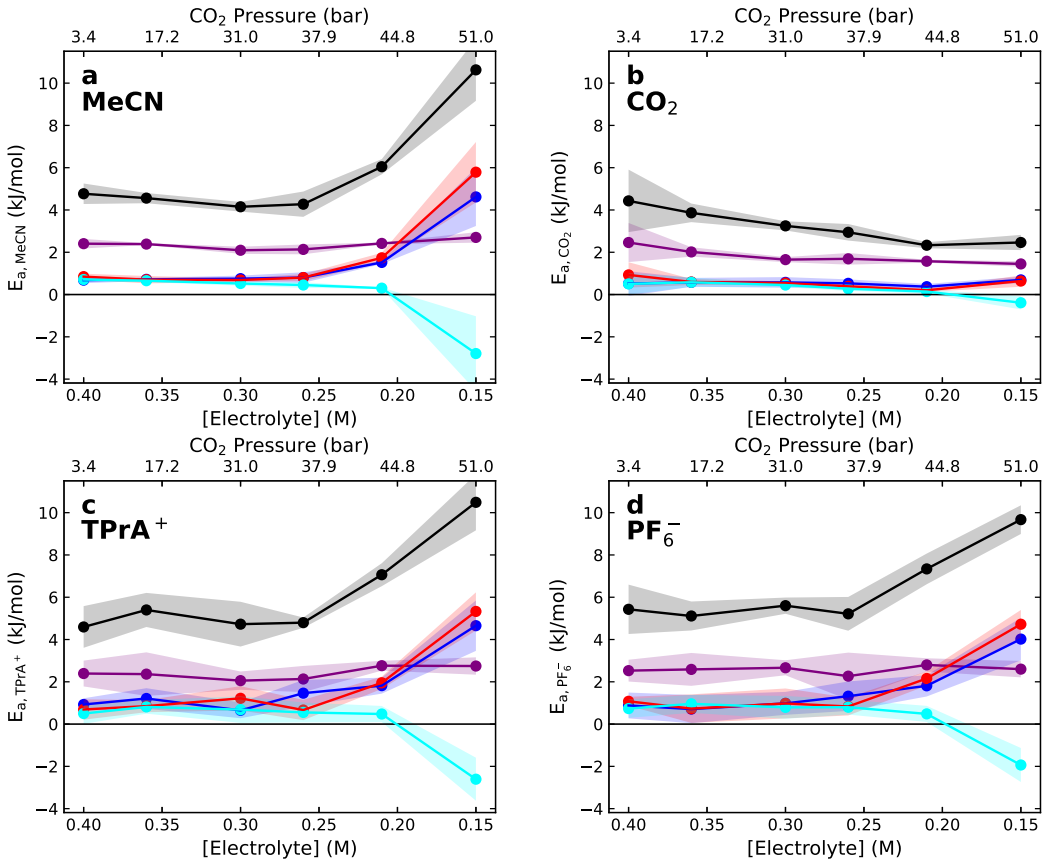


Figure 5: The energetic contributions to the activation energy of diffusion over increasing $CO_2$ pressure/corresponding electrolyte dilution for **a.** MeCN, **b.** $CO_2$, **c.** $PF_6^-$, and **d.** $TPrA^+$. Results are shown for the total activation energy (black) as well as contributions from the kinetic (purple), Lennard-Jones (red), Coulombic (blue), and angle (cyan) energies. Shaded regions indicate 95% confidence intervals.

expansion is well-described by the increase in cation-anion coordination number with increasing $CO_2$ pressure that we have reported previously.[8] The energetic effect of ion-pairing can be understood by decomposing the activation energy into contributions from intermolecular interactions between different types of molecules.

From Eqs. (7) and (8), the contributions to $E_{a,TPrA^+}$ from Coulombic interactions between $TPrA^+$ and $PF_6^-$ were calculated with changing $CO_2$ pressure. These quantities were also calculated for $E_{a,PF_6^-}$ and show similar behavior, which is shown in Fig. S3. The results are presented in Fig. 6, and show that, as $CO_2$ pressure increases, the contribution of the Coulombic interactions between the cation and the anion to $E_{a,TPrA^+}$ increases. Conversely, at the same time, the cation-cation and anion-anion Coulombic interactions have an increasingly negative contribution to $E_{a,TPrA^+}$. This demonstrates how the energetically favorable, oppositely-charged ionic attraction makes diffusion less energetically favorable, and more so at high $CO_2$ pressure where the most ion-pairing is observed. However, this effect is tempered by the ionic repulsion experienced between ions of like-charge, which keeps the overall Coulombic contribution to $E_{a,TPrA^+}$ non-prohibitive to diffusion.

Smaller magnitude intermolecular contributions shed further light on the origin of increased activation energy of diffusion of the ions. The non-zero contributions to $E_{a,TPrA^+}$ from Lennard-Jones and Coulombic interactions between all pairs of molecules are presented in Fig. 7 with changing $CO_2$ pressure. These quantities are again similar to those for $E_{a,PF_6^-}$, which is shown in Fig. S4. The ma-

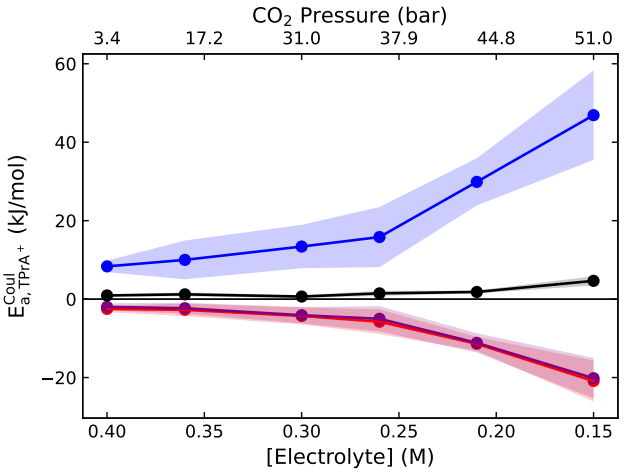


Figure 6: Effect of anion and cation intermolecular Coulombic interactions on the activation energy of diffusion of $TPrA^+$ are shown, along with the total $E^{Coul}_{a,TPrA^+}$ (black). Contributions from the cation-anion (blue), anion-anion (red), and cation-cation (purple) interactions are plotted. Shaded regions indicate 95% confidence intervals.

jor Lennard-Jones intermolecular contributions come from MeCN-MeCN and $CO_2$-$CO_2$ interactions, which each increase with increasing $CO_2$ pressures. Other Coulombic contributions to $E_{a,TPrA^+}$ include positive contributions from MeCN-MeCN, MeCN-$CO_2$, and $CO_2$-$CO_2$ interactions, and negative contributions from MeCN-ion interactions. The absence of contributions from $CO_2$-ion interactions shows the difference in role that the solvating molecules play: MeCN stabilizes diffusing ions, while $CO_2$ neither stabilizes nor destabilizes.

These intermolecular contributions shed light on the mechanism of a diffusing ion, ultimately giving insight to the origin of the solution conductivity loss in CXEs at high $CO_2$ pressure. Fig. 8 provides a schematic of this mechanism, and the following discussion of the activation energy contributions from intermolecular interactions are in line with the proposed mechanism. For solution conductivity to be maintained, an ion must be able to diffuse separately from an oppositely-charged partner. The breaking of the cation-anion Coulombic attraction is the largest contribution to $E_{a,TPrA^+}$, but nearby like-charged ions facilitate diffusion

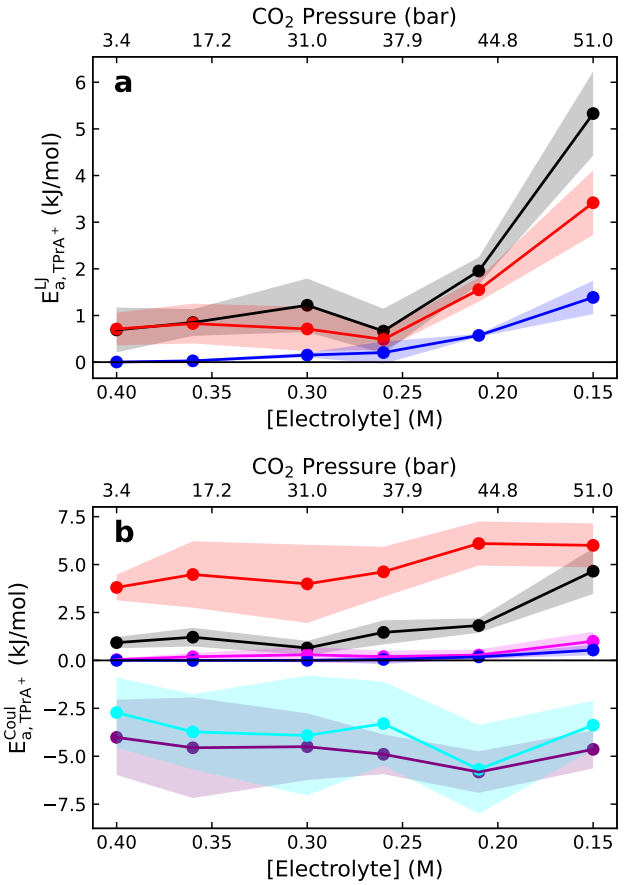


Figure 7: Contributions from intermolecular **a.** Lennard-Jones and **b.** Coulombic interactions to the activation energy of diffusion of $TPrA^+$ are shown, along with the total $E^{LJ}_{a,TPrA^+}$ and $E^{Coul}_{a,TPrA^+}$ (black). Contributions from the MeCN-MeCN (red), $CO_2$-$CO_2$ (blue), MeCN-$CO_2$ (magenta), MeCN-$PF_6^-$ (purple), and MeCN-$TPrA^+$ (cyan) interactions are plotted. Shaded regions indicate 95% confidence intervals.

through Coulombic repulsion.

For the ion to diffuse, it must also break the interactions of the nearby solvation structure, and we see that the positive Lennard-Jones contributions to $E_{a,TPrA^+}$ from MeCN-MeCN and $CO_2$-$CO_2$ interactions show the energetic barrier involves breaking stable solvent-solvent interactions. At high $CO_2$ pressures, these contributions are increased, demonstrating that MeCN and $CO_2$ molecules must move into environments that are less energetically-favorable when there are greater concentrations of $CO_2$. The remaining Coulombic intermolec-

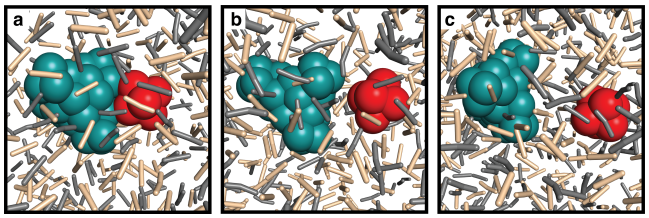


Figure 8: A schematic representation of the diffusion process of $TPrA^+ \cdots PF_6^-$ in the CXE, with MeCN (gray), $CO_2$ (tan), $TPrA^+$ (teal), and $PF_6^-$ (red). In the initial state, Panel **a.**, $TPrA^+$ is ion-paired with $PF_6^-$. For diffusion to occur, the ion must break its ion pair interaction and the surrounding solvent must move out of the way accommodate it. Panel **b.** shows the beginnings of separation, where the ions have a few solvent molecules between them. The final state, Panel **c.**, shows the ions separated by a greater distance and are thus more able to diffuse freely. For simplicity, we have not shown the effect of other ions, which enhance diffusion of ions of like charge through Coulombic repulsion. System visualizations were prepared using PyMOL.[30]

ular contributions show a similar picture, with positive contributions to $E_{a,TPrA^+}$ from MeCN-MeCN, MeCN-$CO_2$ and $CO_2$-$CO_2$ interactions that increase at high $CO_2$ pressures. The contributions from MeCN-ion interactions show the role of MeCN as a stabilizer for a diffusing $TPrA^+$, as well as stabilizing the $PF_6^-$ left behind. This stabilizing effect is diminished at high $CO_2$ pressures, presumably because high concentrations of $CO_2$ dictate fewer MeCN-ion interactions.

The origin of the critical effects of the activation entropy with increasing $CO_2$ pressure are also suggested by Panel b of Fig. 8. Namely, it indicates that the $CO_2$-rich milieu may provide a greater number of ways to arrange the transition state for ion depairing, both structurally and compositionally.

# 6 Conclusion

In this work, a molecular-level understanding of the factors contributing to a loss of solution conductivity in CXEs was developed. From MD simulations of systems corresponding to an experimentally determined range of $CO_2$ pressures and corresponding electrolyte dilution, diffusion coefficients and activation energies of diffusion were calculated.

The introduction of high concentrations of $CO_2$ in the organic electrolyte system has the primary effect of increasing the mobility of all components. $CO_2$ exhibits the highest diffusion coefficient and the most dramatic increase across the pressure range, MeCN has a lower diffusion coefficient at all pressures but still experiences a noticeable increase. The ions each have the lowest diffusion coefficients at all pressures, with that of $PF_6^-$ slightly larger than that of $TPrA^+$, and exhibit a doubling of the diffusion coefficient across the $CO_2$ pressure range.

The activation energies of diffusion were calculated for all species and the values as a function of $CO_2$ pressure are quantitatively similar for MeCN and the ions. They are effectively unchanged below 44.8 bar and then exhibit a sharp increase. In contrast, the diffusion activation energy for $CO_2$ monotonically decreases with $CO_2$ pressure.

The contradictory trends in the MeCN and ion diffusion coefficients and corresponding activation energies demonstrate that the activation entropy plays a dominant role in diffusion at higher $CO_2$ pressures. In contrast, entropic effects are minimal for $CO_2$ diffusion where the behavior is well described by considering the activation energy alone (Fig. S1). The origin of this behavior may be connected to the approach of the solubility limit for the ions in the CXE, suggesting changes in the microenvironment. The diffusion of molecules and mixing between phases in such a system would be entropically favored. Another possible factor could be the entropically unfavored ion-pairing interactions, where the separation of two paired ions would implicate increased diffusion driven by entropy.

At high $CO_2$ pressures, the drop in solution conductivity is driven by increased ion-pairing interactions. The ions experience an increased activation energy of diffusion at high $CO_2$ pressures, with major contributions from Coulombic ion-ion interactions and Lennard-

Jones solvent interactions. As the system becomes mainly composed of $CO_2$ at high pressures, the energetic barrier for an ion to diffuse is made more difficult by the increased activation energy to break the ion-pair interaction, as well as increased activation energy to break the solvent structure surrounding it.

To improve the efficiency of CXEs, electrolyte design may be a powerful avenue to address the decline in solution conductivity with increasing $CO_2$ pressure. We envision that careful choice of ion structure may be applied to tune the dominating ionic interactions elucidated in this work. In particular, the cation-anion Coulombic attraction may be reduced by choosing electrolytes which have larger protecting structures around a charge-dense center, while incorporating features that maintain solubility in the increasingly nonpolar $CO_2$-expanded MeCN solvent.

# Supporting Information

Simulation details, including force field parameters and system compositions at each $CO_2$ pressure; further activation energy decompositions, including for $PF_6^-$.

# 7 Acknowledgments

This work was supported by the US National Science Foundation through awards CHE-2102656 (W.H.T) and CBET-1605524 (J.D.B.). C.K.N. was supported by a U.S. National Science Foundation Research Traineeship (NRT) at the University of Kansas (DGE-1922649). E.R.B. was supported by the Madison & Lila Self Graduate Fellowship at the University of Kansas. The calculations were performed at the University of Kansas Center for Research Computing (CRC), including including the BigJay cluster resource funded through NSF Grant MRI-2117449.

# References

(1) Subramaniam, B. Enhancing the Stability of Porous Catalysts with Supercritical Reaction Media. *Appl. Catal., A* **2001**, *212*, 199–213.

(2) Subramaniam, B. Gas-Expanded Liquids for Sustainable Catalysis and Novel Materials: Recent Advances. *Coord. Chem. Rev.* **2010**, *254*, 1843–1853.

(3) Akien, G. R.; Poliakoff, M. A Critical Look at Reactions in Class I and II Gas-Expanded Liquids using $CO_2$ and Other Gases. *Green Chem.* **2009**, *11*, 1083.

(4) Jessop, P. G.; Subramaniam, B. Gas-Expanded Liquids. *Chem. Rev.* **2007**, *107*, 2666–2694.

(5) Houndonougbo, Y.; Jin, H.; Rajagopalan, B.; Wong, K.; Kuczera, K.; Subramaniam, B.; Laird, B. Phase Equilibria in Carbon Dioxide Expanded Solvents: Experiments and Molecular Simulations. *J. Phys. Chem. B* **2006**, *110*, 13195–13202.

(6) Palafox-Hernandez, J. P.; Mendis, C. H.; Thompson, W. H.; Laird, B. B. Pressure and Temperature Tuning of Gas-Expanded Liquid Structure and Dynamics. *J. Phys. Chem. B* **2019**, *123*, 2915–2924.

(7) Sconyers, D. J.; Shaughnessy, C. I.; Lee, H.; Subramaniam, B.; Leonard, K. C.; Blakemore, J. D. Enhancing Molecular Electrocatalysis of $CO_2$ Reduction with PressureTunable $CO_2$Expanded Electrolytes. *ChemSusChem* **2020**, *13*, 6338–6345.

(8) Nilles, C. K.; Borkowski, A. K.; Bartlett, E. R.; Stalcup, M. A.; Lee, H.-J.; Leonard, K. C.; Subramaniam, B.; Thompson, W. H.; Blakemore, J. D. Mechanistic Basis of Conductivity in Carbon Dioxide-Expanded Electrolytes: A Joint ExperimentalTheoretical Study. *J. Am. Chem. Soc.* **2024**, *146*, 2398–2410.

(9) Stalcup, M. A.; Nilles, C. K.; Lee, H.-J.; Subramaniam, B.; Blakemore, J. D.; Leonard, K. C. Organic Electrosynthesis in $CO_2$-eXpanded Electrolytes: Enabling Selective Acetophenone Carboxylation to Atrolatic Acid. *ACS Sustainable Chem. Eng.* **2021**, *9*, 10431–10436.

(10) Shaughnessy, C. I.; Sconyers, D. J.; Lee, H.-J.; Subramaniam, B.; Blakemore, J. D.; Leonard, K. C. Insights into Pressure Tunable Reaction Rates for Electrochemical Reduction of $CO_2$ in Organic Electrolytes. *Green Chem.* **2020**, *22*, 2434–2442.

(11) Hori, Y.; Kikuchi, K.; Murata, A.; Suzuki, S. Production of Methane and Ethylene in Electrochemical Reduction of Carbon Dioxide at Copper Electrode in Aqueous Hydrogencarbonate Solution. *Chem. Lett.* **1986**, *15*, 897–898.

(12) Ahn, S. T.; Abu-Baker, I.; Palmore, G. T. R. Electroreduction of $CO_2$ on Polycrystalline Copper: Effect of Temperature on Product Selectivity. *Catal. Today* **2017**, *288*, 24–29.

(13) Lwe, A.; Rieg, C.; Hierlemann, T.; Salas, N.; Kopljar, D.; Wagner, N.; Klemm, E. Influence of Temperature on the Performance of Gas Diffusion Electrodes in the $CO_2$ Reduction Reaction. *ChemElectroChem* **2019**, *6*, 4497–4506.

(14) Vos, R. E.; Kolmeijer, K. E.; Jacobs, T. S.; van der Stam, W.; Weckhuysen, B. M.; Koper, M. T. M. How Temperature Affects the Selectivity of the Electrochemical $CO_2$ Reduction on Copper. *ACS Catal.* **2023**, *13*, 8080–8091.

(15) Shaughnessy, C. I.; Sconyers, D. J.; Kerr, T. A.; Lee, H.; Subramaniam, B.; Leonard, K. C.; Blakemore, J. D. Intensified Electrocatalytic $CO_2$ Conversion in PressureTunable $CO_2$Expanded Electrolytes. *ChemSusChem* **2019**, *12*, 3761–3768.

(16) Span, R.; Wagner, W. A New Equation of State for Carbon Dioxide Covering the Fluid Region from the TriplePoint Temperature to 1100 K at Pressures up to 800 MPa. *J. Phys. Chem. Ref. Data* **1996**, *25*, 1509–1596.

(17) Piskulich, Z. A.; Laird, B. B. Molecular Simulations of Phase Equilibria and Transport Properties in a Model $CO_2$-Expanded Lithium Perchlorate Electrolyte. *J. Phys. Chem. B* **2021**, *125*, 9341–9349.

(18) Mesele, O. O.; Thompson, W. H. Removing the Barrier to the Calculation of Activation Energies. *J. Chem. Phys.* **2016**, *145*, 134107.

(19) Piskulich, Z. A.; Mesele, O. O.; Thompson, W. H. Removing the Barrier to the Calculation of Activation Energies: Diffusion Coefficients and Reorientation Times in Liquid Water. *J. Chem. Phys.* **2017**, *147*, 134103.

(20) Piskulich, Z. A.; Mesele, O. O.; Thompson, W. H. Activation Energies and Beyond. *J. Phys. Chem. A* **2019**, *123*, 7185–7194.

(21) Tolman, R. C. Statistical Mechanics Applied to Chemical Kinetics. *J. Am. Chem. Soc.* **1920**, *42*, 2506–2528.

(22) Truhlar, D. G. Interpretation of the Activation Energy. *J. Chem. Educ.* **1978**, *55*, 309.

(23) Bernstein, R. B.; Levine, R. D. *Molecular Reaction Dynamics and Chemical Reactivity*; Oxford University Press: New York, 1987; pp 181–190.

(24) Edwards, D. M.; Madden, P. A.; McDonald, I. R. A Computer Simulation Study of the Dielectric Properties of a Model of Methyl Cyanide: I. The Rigid Dipole Case. *Mol. Phys.* **1984**, *51*, 1141–1161.

(25) Harris, J. G.; Yung, K. H. Carbon Dioxide's Liquid-Vapor Coexistence Curve

And Critical Properties as Predicted by a Simple Molecular Model. *J. Phys. Chem.* **1995**, *99*, 12021–12024.

(26) Ryckaert, J.-P.; Ciccotti, G.; Berendsen, H. J. Numerical Integration of the Cartesian Equations of Motion of a System with Constraints: Molecular Dynamics of *n*-Alkanes. *J. Comput. Phys.* **1977**, *23*, 327–341.

(27) Wang, J.; Wolf, R. M.; Caldwell, J. W.; Kollman, P. A.; Case, D. A. Development and Testing of a General Amber Force Field. *J. Comput. Chem.* **2004**, *25*, 1157–1174.

(28) Liu, Z.; Wu, X.; Wang, W. A Novel United-Atom Force Field for Imidazolium-Based Ionic Liquids. *Phys. Chem. Chem. Phys.* **2006**, *8*, 1096–1104.

(29) Plimpton, S. Fast Parallel Algorithms for Short-Range Molecular Dynamics. *J. Comput. Phys.* **1995**, *117*, 1–19.

(30) The PyMOL Molecular Graphics System, Version 3.0 Schrdinger, LLC.

(31) Darden, T.; York, D.; Pedersen, L. Particle Mesh Ewald: An $N$ log( $N$ ) Method for Ewald Sums in Large Systems. *J. Chem. Phys.* **1993**, *98*, 10089–10092.

(32) Pollock, E.; Glosli, J. Comments on P3M, FMM, and the Ewald Method for Large Periodic Coulombic Systems. *Comput. Phys. Commun.* **1996**, *95*, 93–110.

(33) Nosé, S. A Unified Formulation of the Constant Temperature Molecular Dynamics Methods. *J. Chem. Phys.* **1984**, *81*, 511–519.

(34) Hoover, W. G. Canonical Dynamics: Equilibrium Phase-Space Distributions. *Phys. Rev. A* **1985**, *31*, 1695–1697.

(35) Shoemaker, D. P.; Garland, C. W.; Steinfeld, J. I. *Experiments in Physical Chemistry*, 3rd ed.; McGraw-Hill: New York, 1974; pp 47–54.

(36) Cohen, S. R.; Plazanet, M.; Rols, S.; Voneshen, D. J.; Fourkas, J. T.; Coasne, B. Structure and Dynamics of Acetonitrile: Molecular Simulation and Neutron Scattering. *J. Mol. Liq.* **2022**, *348*, 118423.

(37) Gurdia, E.; Pinzn, R.; Casulleras, J.; Orozco, M.; Luque, F. J. Comparison of Different Three-site Interaction Potentials for Liquid Acetonitrile. *Mol. Simul.* **2001**, *26*, 287–306.

(38) Houndonougbo, Y.; Laird, B. B.; Kuczera, K. Transport Properties of $CO_2$-Expanded Acetonitrile from Molecular Dynamics Simulations. *J. Chem. Phys.* **2007**, *126*, 074507.

(39) Mariani, A.; Bonomo, M.; Wu, B.; Centrella, B.; Dini, D.; Castner, E. W.; Gontrani, L. Intriguing Transport Dynamics of Ethylammonium NitrateAcetonitrile Binary Mixtures Arising from Nano-Inhomogeneity. *Phys. Chem. Chem. Phys.* **2017**, *19*, 27212–27220.

(40) Arkhipova, E. A.; Ivanov, A. S.; Levin, M. M.; Maslakov, K. I.; Kupreenko, S. Y.; Savilov, S. V. Study of Tetraalkylammonium Salts in Acetonitrile Solutions: Transport Properties, Density, Thermal Expansion and Phase Transitions. *J. Mol. Liq.* **2022**, *367*, 120536.

(41) Norton, C. D.; Thompson, W. H. On the Diffusion of Acetonitrile in Nanoscale Amorphous Silica Pores. Understanding Anisotropy and the Effects of Hydrogen Bonding. *J. Phys. Chem. C* **2013**, *117*, 19107–19114.

(42) Gee, P. J.; Van Gunsteren, W. F. Acetonitrile Revisited: a Molecular Dynamics Study of the Liquid Phase. *Mol. Phys.* **2006**, *104*, 477–483.

(43) Hurle, R. L.; Woolf, L. A. Self-Diffusion in Liquid Acetonitrile Under Pressure. *J. Chem. Soc., Faraday Trans. 1* **1982**, *78*, 2233.

(44) Borkowski, A. K.; Piskulich, Z. A.; Thompson, W. H. Examining the Hofmeister Series through Activation Energies: Water Diffusion in Aqueous Alkali-Halide Solutions. *J. Phys. Chem. B* **2021**, *125*, 350–359.

(45) Piskulich, Z. A.; Borkowski, A. K.; Thompson, W. H. A Maxwell Relation for Dynamical Timescales with Application to the Pressure and Temperature Dependence of Water Self-Diffusion and Shear Viscosity. *Phys. Chem. Chem. Phys.* **2023**, *25*, 12820–12832.

# TOC Graphic

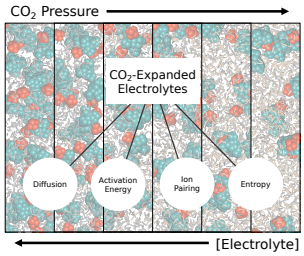
$CO_2$ Pressure
$CO_2$-Expanded Electrolytes
Diffusion
Activation Energy
Ion Pairing
Entropy
[Electrolyte]